Appl. Phys. A 90, 581–589 (2008)
DOI: 10.1007/s00339-007-4336-7

Applied Physics A
Materials Science & Processing

A.K. CHAUHAN[1]
D.K. ASWAL[1,✉]
S.P. KOIRY[1]
S.K. GUPTA[1]
J.V. YAKHMI[1]
C. SÜRGERS[2]
D. GUERIN[3]
S. LENFANT[3]
D. VUILLAUME[3]

Self-assembly of the 3-aminopropyltrimethoxysilane multilayers on Si and hysteretic current–voltage characteristics

[1] Technical Physics and Prototype Engineering Division, Bhabha Atomic Research Centre, Mumbai 400085, India
[2] Physikalisches Institut and Center for Functional Nanostructures, Universität Karlsruhe, 76128 Karlsruhe, Germany
[3] Molecular Nanostructures and Devices Group, Institut d'Electronique, Microelectronique et Nanotechnologie – CNRS, BP 60069, avenue Poincaré, 59652 Villeneuve d'Ascq Cedex, France

Received: 2 July 2007/Accepted: 16 October 2007
Published online: 24 November 2007 •

ABSTRACT We report the deposition of 3-aminopropyltrimethoxysilane (APTMS) multilayers on $SiO_x/Si(p^{++})$ substrates by a layer-by-layer self-assembly process. The multilayers were grafted in a glove box having nitrogen ambient with both humidity and oxygen contents < 1 ppm using APTMS solutions prepared in an anhydrous toluene. Deposition of the multilayers has been carried out as a function of solution concentration and grafting time. Characterization of the multilayers using static de-ionized water contact angle, ellipsometry, X-ray photoelectron spectroscopy and atomic force microscope measurements revealed that self-assembling of the multilayers takes place in two distinct stages: (i) the first APTMS monolayer chemisorbs on a hydroxylated oxide surface by a silanization process and, (ii) the surface amino group of the first monolayer chemisorbs the hydrolyzed silane group of other APTMS molecules present in the solution, leading to the formation of a bilayer. The second stage is a self-replicating process that results in the layer-by-layer self-assembly of the multilayers with trapped NH_3^+ ions. The current–voltage characteristics of the multilayers exhibit a hysteresis effect along with a negative differential resistance, suggesting their potential application in the molecular memory devices. A possible mechanism for the observed hysteresis effect based on filling and de-filling of the NH_3^+ acting as traps is presented.

PACS 73.30.+y

1 Introduction

Recent worldwide research on self-assembled monolayers (SAMs) on silicon substrates has witnessed a tremendous potential through demonstrations of various molecular electronic devices, such as, rectifiers, memories, resonant tunnel diodes etc. [1–5]. Consequently, molecular electronics is being considered to be one of the possible solutions to the scaling limit problem that the semiconductor industry may have to face in the next decade [6]. The most common and successful route for the deposition of SAMs on Si substrates is through silanization process [7, 8]. In this process, SAMs are formed spontaneously by immersing the OH-terminated SiO_x/Si substrates into an active solution e.g. surfactant molecules $R(CH_2)_nSiX_3$ ($X = Cl$, OCH_3 or OC_2H_5; R = surface group e.g. CH_3, NH_2, SH, $CH{=}CH_2$ etc.) dissolved in an appropriate solvent (usually aliphatic and aromatic hydrocarbons). Alternatively, the high vapor pressure silane molecules can also be deposited on OH-terminated SiO_x/Si substrates by vapor phase [1]. The mechanism of SAM formation during the silanization process is well established, which is known to take place in four steps [1, 7, 8]. The first step is physisorption, in which the silane molecules get physisorbed at the hydrated silicon surface. In the second step, the silane head-groups (SiX_3) arriving close to the substrate hydrolyzes, in the presence of the adsorbed water layer on the surface, into highly polar silanetriol $Si(OH)_3$. In the third step, these polar $Si(OH)_3$ groups form covalent bonds with the silanol groups (Si−OH) on substrate surface and with the silanol groups from neighboring molecules by creating a polysiloxane network in the plane of the substrate. During the initial period, only a few molecules will chemisorb (by steps 1–3) on the substrate surface and the monolayer is expected to be in a disordered (or liquid) state. However, at longer times, the surface coverage eventually reaches the point where a well-ordered and compact monolayer is obtained (step 4). The self-organization is driven by van der Waals interactions among the linear alkyl-chains. The kinetics of the SAMs monolayer formation has also been investigated by scanning probe microscopy [9–11]. It has been found that the growth kinetics depends on the alkyl-chain length: long chains grow via 2D island nucleation and growth mechanisms, while the short chains exhibit layered growth behavior [1]. This has been attributed to the chain length dependent chemisorption and diffusion rates of molecules on the substrate surface, which are known to decrease with increasing chain length [11].

For the development of molecular electronic devices, high-quality SAMs of both short as well as long alkyl-chains are needed. For instance, SAMs of long alkyl-chains (number of C atoms > 18) are needed for the gate dielectric in field-effect molecular transistors [12, 13]; while short SAMs of alkyl-chains (number of C atoms 3–6) are desirable for

✉ Fax: +91-22-25505296, E-mail: dkaswal@yahoo.com

resonant tunnel diodes [1, 14] based on σ–π–σ molecular architecture. SAMs of different chain lengths, i.e. upto number of C atoms = 18, have successfully been grafted on Si surfaces via silanization process, as discussed above. However, SAMs of longer chain lengths (number of C atoms > 18) are found to be highly disordered due to the mingling of the chains [1]. Thus, deposition of high quality molecular films with high thickness by a single step silanization process is in general difficult to obtain. In order to deposit molecular films of a predetermined thickness, Maoz et al. [15, 16] have pioneered a layer-by-layer self-assembly process in which discrete monolayers are sequentially deposited on a substrate.

In this paper, we present deposition of 3-aminopropyltrimethoxysilane [APTMS: $NH_2(CH_2)_3Si(OCH_3)_3$], multilayers of controlled thickness on SiO_x/Si substrates using the layer-by-layer self-assembly process. It may be noted here that a large numbers of investigations on the self-assembly of the APTMS monolayer and multilayer have been reported in the literature [17–22]. While deposition of high-quality APTMS monolayers have been reported by several groups, the quality of the multilayers was poor. It has been found that the surface coverage and structure of the APTMS multilayers depends sensitively on various experimental parameters, such as, choice of solvent, water content of the solvent, silane concentration and reaction time [17–22]. We have optimized these parameters to obtain the high-quality APTMS multilayers. The self-assembly process of the deposited APTMS multilayers has been envisaged using the data obtained from the various characterization techniques, namely, static de-ionized water contact angle measurements, ellipsometry, X-ray photoelectron spectroscopy (XPS) and atomic force microscopy (AFM). The current–voltage (J–V) characteristics of the multilayers of different thickness have been measured. It has been demonstrated for the first time that APTMS multilayer having ≥ 4 layers exhibits hysteretic J–V loops with a negative differential resistance (NDR) region, suggesting their potential application in the molecular memory devices. This effect has been explained using filling and de-filling of the $NH_3{}^+$ traps.

2 Experimental

The 3-aminopropyltrimethoxysilane (APTMS) used was obtained from Gelest. Chloroform (extra pure grade) was obtained from Scharlau, and n-hexane (99% ACS grade from Carlo Erba) was distilled over calcium hydride prior to use. Hydrogen peroxide (30% in water), sulfuric acid (98%), anhydrous p-xylene (99%) and anhydrous toluene (99.8%) were obtained from Aldrich and used as received without further purification. Hydrofluoric acid (50% VLSI grade) was purchased from Merck. The precut heavily doped Si(p^{++}) substrates purchased from Siltronix (resistivity: $< 10^{-3}\ \Omega$ cm and approximate size: 2×1 cm^2) having a native oxide (SiO_x) of 16 Å thickness were ultrasonically cleaned in acetone and chloroform, rinsed by de-ionized water and dried in a stream of nitrogen. The native oxide layer was removed by dipping the substrate into HF (30%) for one minute. A hydrophobic character of the substrate surface indicated that the native oxide had been etched out. These substrates were then dipped into a freshly prepared hot (temperature $\sim 120\,^\circ$C) piranha solution [$H_2O_2 : H_2SO_4$ in a ratio 1 : 2 (v/v)] for 30 min. During this treatment, the formation of a fresh SiO_2 layer takes place at the Si surface. The measured thickness of this SiO_2 layer was 13 Å. A thorough cleaning of these substrates were carried out by rinsing in de-ionized water followed by drying in a stream of nitrogen. The process of rinsing and drying was repeated 5–6 times to remove any traces of acid from the surface. A very small static de-ionized water contact angle ($< 2^\circ$) of these surfaces revealed their hydrophilic character owing to the fact that the SiO_2 surface is terminated with hydroxyl groups. Immediately after the cleaning, these substrates were transferred into a glove box having N_2 ambient with both humidity and oxygen contents of < 1 ppm. Among various anhydrous solvents, i.e. n-hexane, toluene, and p-xylene, used for making APTMS solution, the anhydrous toluene was found to yield uniform grafting of APTMS on the substrates. In order to deposit controlled thickness of the self-assembled APTMS multilayers, following two sets of experiments were carried out.

(i) The concentration of APTMS in anhydrous toluene was varied between 2.5×10^{-7} to 2×10^{-2} (v/v). Piranha cleaned substrates were carefully placed inside the solution for a fixed duration of 30 min to determine the optimum concentration for the deposition of APTMS monolayer.

(ii) The thickness of the grafted APTMS layers was measured as a function of grafting time using a solution of the 2×10^{-3} (v/v) concentration.

In all the experiments, immediate after the removal of substrates from the solution, they were ultrasonically cleaned in chloroform for 5 min, essentially to remove physisorbed molecules at the surface, rinsed several times in de-ionized water, blow-dried with nitrogen and stored in a dust-free nitrogen atmosphere.

All the self-assembled APTMS samples were characterized by various techniques. The information on the surface group was ascertained by de-ionized (DI) water contact angle measurement using a contact angle meter (Digidrop, GBX, France) system. The thickness of the samples was measured using spectroscopic ellipsometer UVSIL (Horiba). The X-ray photoelectron spectroscopy (XPS) of the samples was carried out using an Mg K_α source (RIBER MBE system) to determine the chemical state of the nitrogen. X-ray diffraction (XRD) patterns of the samples ware recorded using Cu K_α radiation. The area analyzed by XPS was ~ 2 mm^2 and, the binding energy scale was calibrated to Au $4f_{7/2}$ line of 83.95 eV. The surface morphology of the samples was imaged using atomic force microscopy (AFM) (Dimension 3100, Digital Instruments). For the electrical characterization, metal/APTMS-layer/Si(p^{++}) structure was completed by using a very small drop of liquid mercury as a counterelectrode. The contact area was calculated after digitizing the side view of Hg drop using a high-resolution camera and measuring the diameter of contact surface of the substrate with Hg. The J–V characteristics were recorded in a dark box using HP4140 (pA meter – dc voltage source).

3 Results and discussion

Figure 1 shows the thickness variation of the self-assembled APTMS layers as a function of solution concentra-

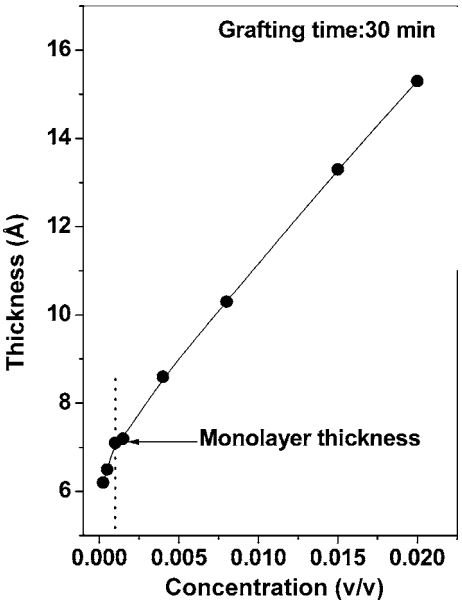

FIGURE 1 Thickness variation of the self-assembled APTMS layers on SiO_2/Si substrates as a function of solution concentration. The grafting time was kept fixed for 30 min and the grafting was carried at room temperature

tion for a fixed grafting period of 30 min. It is apparent that from a solution of the concentration of 2×10^{-3} (v/v), the thickness of the grafted APTMS layer is 7 Å, which is nearly equal to the theoretical length of the APTMS molecule, indicating formation of a well organized monolayer. However, for higher solution concentration, the thickness data suggest formation of the multilayers. Typical AFM images of the samples prepared using solutions of the concentrations of 2×10^{-3} and 2×10^{-2} (v/v) are shown in Fig. 2. The height profile data indicate that the sample grafted from a solution of the concentration of 2×10^{-3} (v/v) has a uniform coverage of the substrate with a surface roughness < 1 Å, while at high solution concentrations samples of highly non-uniform morphology, consisting of mounds of varying heights (upto a max. height of 28 Å), are deposited. The measured DI water contact angles on these two samples (within 10 min after their preparation) were, respectively, < 15 and $\sim 40°$. The NH_2 group is hydrophilic in character. Thus a low contact angle ($< 15°$), along with a measured thickness of 7 Å and surface roughness < 1 Å, suggests that samples prepared from a solution of the concentration of 2×10^{-3} (v/v) are well organized monolayers terminated with a NH_2 group. It may be noted here that the reported water contact angles for NH_2-terminated surfaces vary widely between 15° and 68° [18, 19]. This discrepancy could be due to the following two reasons.

(i) The contact angle measurements are made at different times after the SAM deposition [21, 22]. This is because the NH_2 group being chemically active could adsorb impurities from the atmosphere, which might be hydrophobic.

(ii) A high surface roughness of the sample [23]. In this case, a certain fraction of the hydrophobic alkyl-chain is exposed at the surface.

In the case of samples prepared from a high concentration solution (2×10^{-2} (v/v)), a high contact angle ($\sim 40°$) indicated that the surface is rough, which is in agreement with the AFM results.

In order to deposit APTMS multilayers of controlled thickness, Si substrates were dipped for different durations

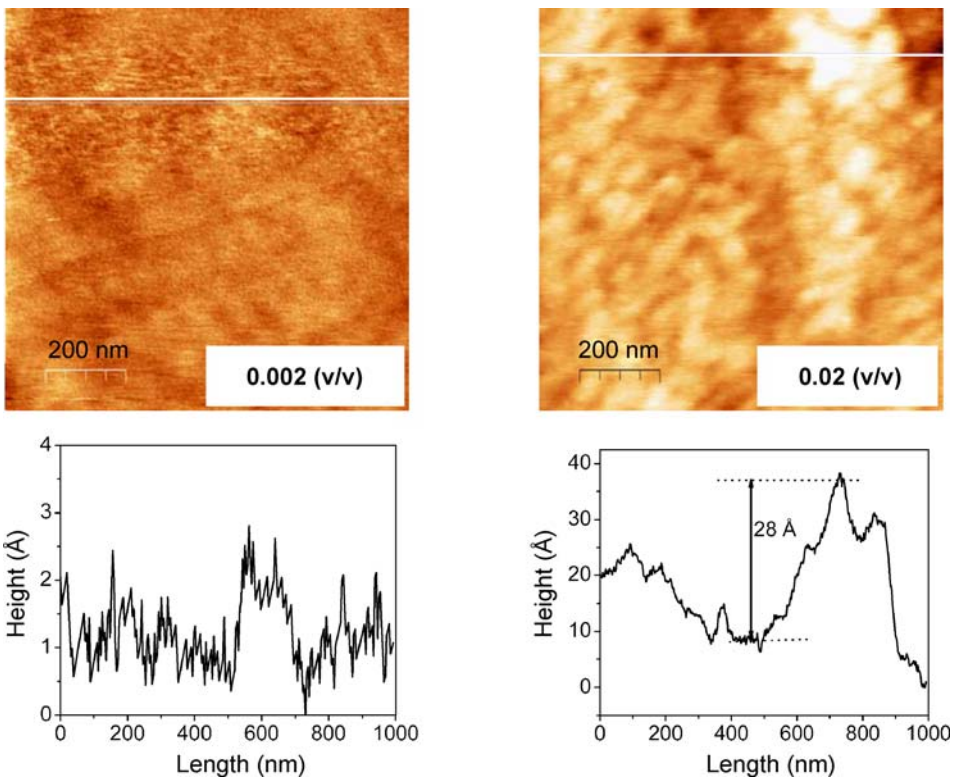

FIGURE 2 1 μm × 1 μm AFM images of APTMS layers deposited using solutions of different concentrations. The height profiles across the *white line* drawn in the respective AFM image are also plotted

in the solution of 2×10^{-3} (v/v) concentration. The variation of the multilayer thickness with grafting time is plotted in Fig. 3. The inset of Fig. 3 reveals that while the first monolayer forms in a period of 30 min, formation of the bilayer (thickness $\sim$ 14 Å) takes a much longer time i.e. $\sim$ 300 min. However, the self-assembly time for the subsequent layers is much longer.

The DI water contact angles measured on different APTMS layers measured within 10 min of their preparation are summarized in Table 1. It is seen that the contact angle for APTMS samples having up to 4-layer remains $< 15°$. This result suggests that the surfaces of these samples are terminated with an NH_2 group. However, for samples with higher number of APTMS layers, the contact angle has high values e.g. for 12-layered APTMS sample the value of contact angle is 42°, indicating tilting of alkyl-chains.

Typical N 1*s* and Si 2*p* XPS spectra recorded for the monolayer and 12-layered APTMS samples are shown in Fig. 4. It is seen that for a monolayer only a single peak at $\sim$ 400.3 eV appears, which corresponds to nitrogen in the NH_2 group [19, 21]. However, for multilayers the N 1*s* peak is very broad, which could be easily deconvoluted into two Gaussian peaks appearing at the binding energy of 400.4 eV and 402.2 eV. The low binding energy peak (400.4 eV) could be due to the nitrogen in the NH_2 group and/or some other bonding, while the second peak (402.2 eV) has been attributed to the presence of an hydrogen-bonded amine or positively charged quaternary nitrogen of the form $-NH_3^+$ [19, 24, 25]. The intensity of the high binding energy peak was found to increase with increasing number of APTMS layers in the sample. This suggests that the formation of $-NH_3^+$ ions is associated with the formation process of the self-assembled multilayers. The Si 2*p* XPS spectra recorded for the monolayer consists of two peaks at 99 eV and 103.3 eV corresponding to respectively, Si and SiO_2, which are expected to originate from the substrates [26].

Typical AFM images of various APTMS samples are shown in Fig. 5. From the height profile of a partial-monolayer, formed after a grafting time of 20 min, it is apparent that the monolayer grows via the 2D nucleation and growth mode. The height of the island is $\sim$ 7 Å, which corresponds to the

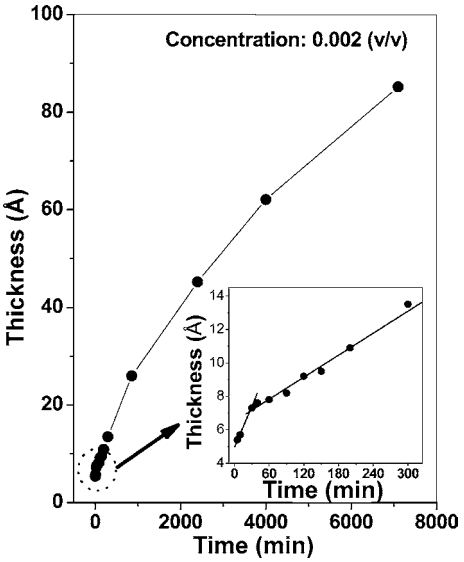

FIGURE 3 Thickness variation of the self-assembled APTMS layer on SiO_2/Si substrates as a function of the grafting time. The solution concentration was kept fixed at 0.002 (v/v)

No. of layers (estimated from ellipsometry measurements)	Contact angle (°)
1	< 10
2	< 15
4	< 15
8	31
10	40
12	42

TABLE 1 Static DI water contact angles for APTMS samples grafted by self assembly

theoretical length of the APTMS molecule. This result is not in agreement with the reported literature, where the short alkyl-chains are found to grow by the layered growth mechanism [1]. This difference could arise due to several factors, such as, different conditions of the substrate surface, different solution concentration, different head group of the silane molecule, and deposition under different ambient conditions. Clearly more research needs to be done to understand the

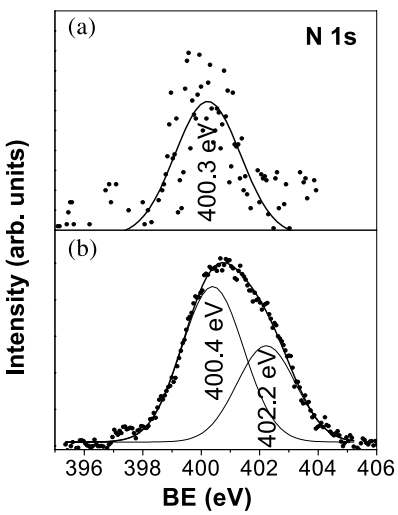

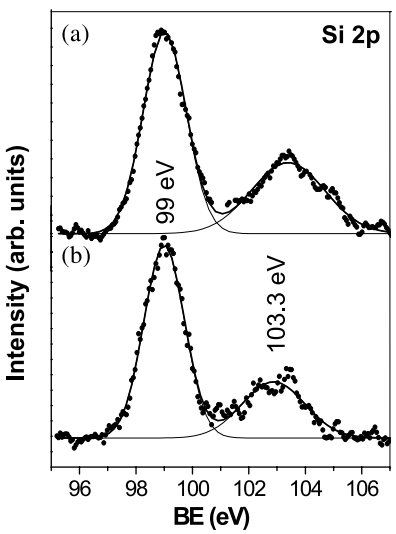

FIGURE 4 N 1*s* and Si 2*p* XPS spectra recorded for (**a**) monolayer and (**b**) 12-layered APTMS sample. The peak values were obtained by fitting the data using Gaussian curve(s)

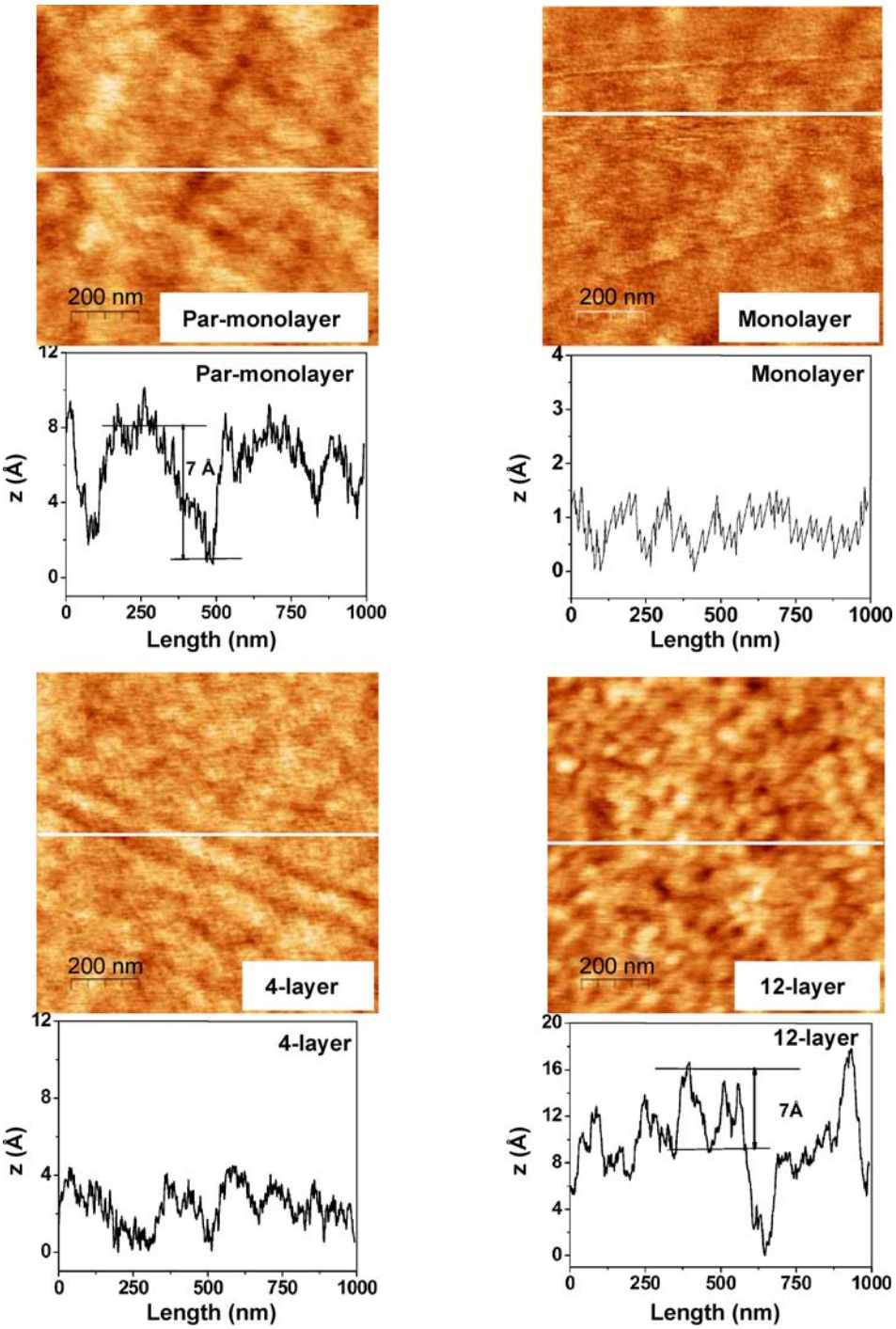

FIGURE 5 1 μm × 1 μm AFM images recorded for different APTMS layers and the height profiles across the *white line* drawn in the respective AFM image

grafting mechanism of the monolayer as a function of these parameters.

The APTMS monolayer attains a surface roughness of < 1 Å, indicating that monolayer has a uniform coverage of the substrate. However, the surface roughness increases with increasing number of layers in the APTMS sample. In addition, the surface morphology also changes. For instance, the morphology of a 12-layered APTMS sample consists of islands having a lateral dimension of 100–200 nm with a height of ~ 7 Å. Such a surface morphology could arise due to the folding of the alkyl-chains, and this inference is well supported by the contact angle data.

In the literature, various possible interactions, marked by 1–7 in Fig. 6a, occurring at the OH-terminated SiO_2 surface when dipped into an APTMS solution have been proposed and these are summarized below. Process (1): the APTMS molecule after undergoing hydrolysis gets chemisorbed on SiO_2 surface by reacting with OH groups (as described in the introduction), resulting in the formation of a monolayer. The terminating NH_2 group of APTMS might get protonated by deionized H_2O (pH 5) or by the slight acidity of the halogenated solvent (chloroform) to form NH_3^+ ions [21, 25]. Process (2): the terminating NH_2 group of APTMS might react with CO_2 from the ambient atmosphere, resulting in the

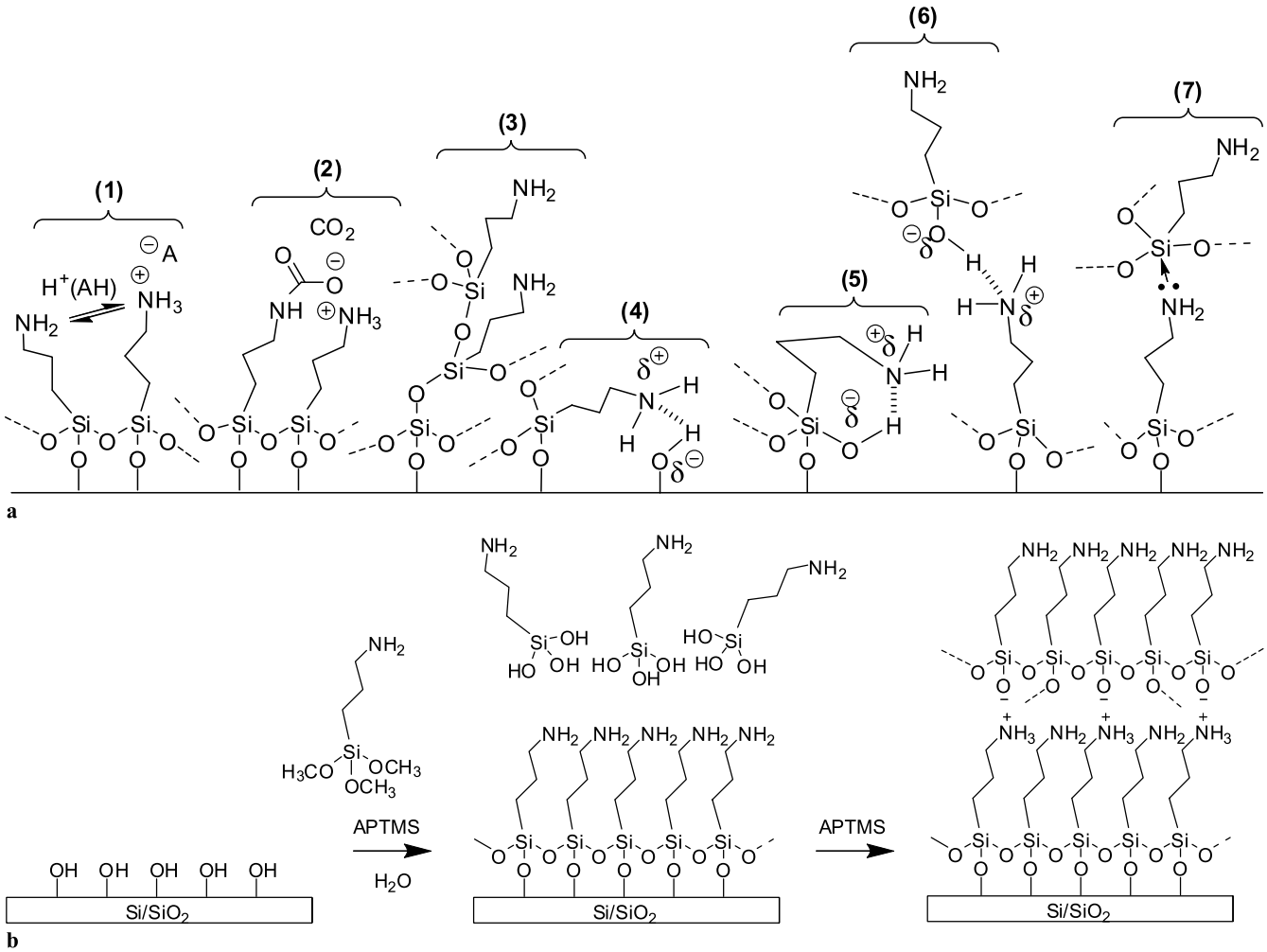

FIGURE 6 (**a**) Various possible mechanisms (1)–(7) that can occur at the OH-terminated SiO_2 surface dipped into a APTMS solution, and (**b**) an ideal self-assembly mechanism of APTMS bilayer formation based on our studies

formation of alkylammonium carbamate [27]. Process (3): the APTMS monolayer might undergo a vertical polymerization through covalent bonded (Si−O−Si polysiloxane reticulation out of the plane of the substrate). This vertical polymerization is favored by the hydrogen bonding between $-NH_2$ groups and Si−OH groups on the hydroxylated surface (4) and intramolecularly within the hydrolyzed molecule itself (5) [28]. Process (6): the head-groups of the hydrolyzed APTMS molecules, $Si(OH)_3$, in the presence of adsorbed water layer, might interact with the surface NH_2 groups of the monolayer. In the literature, this interaction is widely described either as a hydrogen bond or as an ionic bond resulting from an acid–base type reaction, considering that a proton transfer occurs from weakly acidic silanol group to basic amino group. Reported pK_a values for surface silanol groups are generally less than 9 and thus lower than pK_a of the acid–base couple RNH_3^+/RNH_2 (in the range 10–11). These values lead to the acid–base equilibrium: $Si{-}OH + NH_{2-} \rightleftarrows Si{-}O^{-}\bullet\bullet\bullet{}^{+}NH_{3-}$. Whatever the mechanism, process (6) results in the layer-by-layer self-assembly of multilayers with the formation of more or less $^{+\delta}NH_{3-}$ charged species. A polycondensation reaction via formation of the Si−O−Si network in the plane of the substrate accompanies the ionic interaction and reinforces the assembly. Process (7): pentacoordinated silicon resulting from the interaction with the NH_2-group can also be present in the molecular film.

We analyze the applicability of the above processes to the formation of the APTMS multilayers in the present case. Process (1) does occur as we have a strong XPS evidence of the formation of the NH_3^+ ions. Process (2) is unlikely in our case, as the samples were prepared under CO_2 free ambient. The vertical polymerization, process (3), as well as the lateral hydrogen bonding with the silanol groups, processes (4) and (5), would result in a highly non-uniform morphology with mounds of different heights. Considering the fact that our samples have a maximum non-uniformity of ~ 7 Å, this indicates that processes (4) and (5) are negligible in the present case. Processes (6) and (7) can take place in our case, as we have shown from XPS data. Therefore, an ideal formation mechanism of APTMS multilayer is presented in Fig. 6b, which consists of two distinct stages. In the first stage, well organized monolayers of APTMS forms. In the second stage, the bilayer formation takes place by formation of Si−O−Si covalent bonds through $Si{-}O^{-}\bullet\bullet\bullet{}^{+}NH_{3-}$ interactions. The second stage is a self-replicating reaction, resulting in the formation of the APTMS multilayers. Since the NH_2 is the

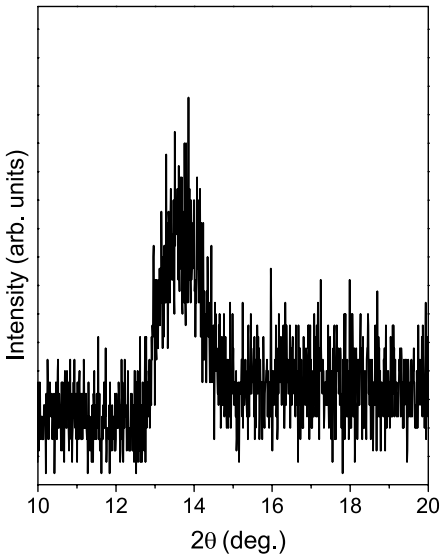

FIGURE 7 The XRD pattern of an APTMS multilayer

surface-group, therefore one can expect that $-NH_3^+$ are located at a regular distance of ~ 7 Å and an increasing concentration of these ions with an increasing number of layers in the APTMS sample. The XRD pattern recorded for the multilayers, as shown in Fig. 7, exhibits a Bragg peak at 13.7°. The calculated interlayer spacing comes out to be 6.4 Å, which is nearly the same as the theoretical length of the APTMS molecule, confirming the layer-by-layer self-assembly of the multilayer. The data shown in the inset of Fig. 2, demonstrates that the kinetics of the first stage of the self-assembly is much faster than that of the second stage. Subsequent attachment of the layer becomes progressively slower as the concentration of the solution depletes.

We have measured the J–V characteristics of the APTMS samples, essentially to investigate that how the presence of NH_3^+ ions modify the electrical transport properties. Typical J–V characteristics of various APTMS samples recorded are shown in Fig. 8. The voltage bias was scanned as $-V_{max} \rightarrow 0\,V \rightarrow +V_{max} \rightarrow 0\,V \rightarrow -V_{max}$, and the scan speed was 5 mV/s. It is seen that the monolayer does not exhibit hysteresis, and the monolayer was found to undergo an electrical breakdown for a bias > 1.7 V (not shown here). A rectification (defined as $J_{+1.5\,V}/J_{-1.5\,V}$) of ~ 6 is attributed to a difference between the work functions of the two electrodes i.e. Hg and Si(p^{++}) [14, 32]. A large current is observed for a positive bias applied on the electrode with the smaller work function (here Hg: ~ 4.5 eV compared to ~ 5.2 eV for Si(p^{++})). The J–V characteristics of APTMS multilayers, in the negative bias region, exhibits a hysteresis along with a negative differential resistance (NDR) region i.e. a decrease in current with increasing voltage. Both these effects are seen to enhance with an increasing number of APTMS layers in the sample. The peak-to-valley ratio of the NDR region, apart from the number of APTMS layer, was found to increase with the value of applied $+V_{max}$. However, if J–V were recorded for $\pm V_{max} < 1.2$ V then no hysteresis was observed, implying that a bias greater than a threshold value of ~ 1.2 V is essential for observing a hysteresis effect. From these non-hysteretic J–V curves (recorded in the bias range between -1.2 V to $+1.2$ V), the value of J at $+1$ V is plotted against the thickness (t) of the multilayers in Fig. 8. The tunneling mechanism of electron transport predicts the variation of J with t by the expression: $J = J_0 e^{-\beta t}$, where β is the tunneling decay parameter having a value of 0.5–1 /Å for alkyl-chains (or even slightly higher) [33]. As seen in Fig. 9, a semilog plot of J as a function of t does not fit to a straight line, indicating that tunneling is not the transport mechanism in the present case for multilayers. For comparison, we have also plotted the theoretical data obtained by assuming $\beta = 0.5$ /Å and $J_0 = 2.6 \times 10^{-2}$ A/cm^2. The value of J_0 was determined by normalizing the theoretical value obtained for the mono-

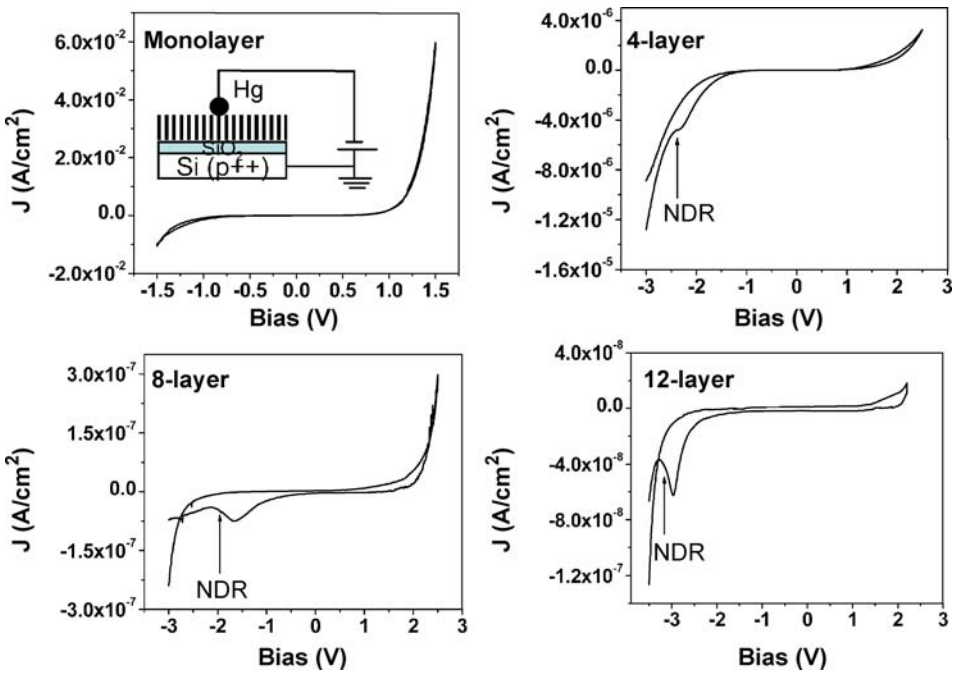

FIGURE 8 Current–voltage (J–V) characteristics recorded for different APTMS samples by scanning the applied bias in the sequence: $-V_{max} \rightarrow 0\,V \rightarrow +V_{max} \rightarrow 0\,V \rightarrow -V_{max}$. The *inset* shows the schematic of the device structure used for the J–V measurements

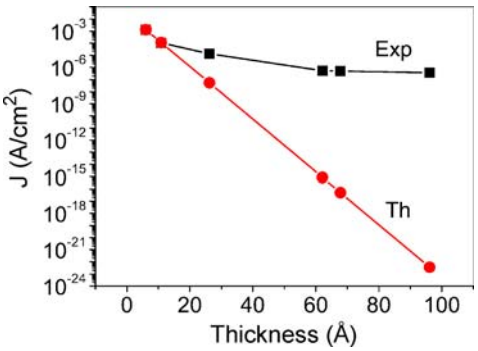

FIGURE 9 Semilog plot of J_{exp} (measured at +1 V using non-hysteretic J–V curves) as a function of the multilayer thickness (t). Also shown is the calculated theoretical current density (J_{th}) using tunneling expression: $J = J_0 e^{-\beta t}$, assuming the value of $\beta = 0.5$ /Å, and $J_0 = 2.6 \times 10^{-2}$ A/cm^2

layer, as the J–V data of the monolayer was found to obey the tunneling mechanism [14]. It is evident from Fig. 9 that the experimental $J_{+1\ V}$ value for the multilayers (> 4 layers) is higher by several orders of magnitude than that predicted using the tunneling $J(t)$ expression.

Since the first report by Tao [34], NDR effects in the molecular junction have been observed in several experiments and several mechanisms have been put forward to explain it. These include: resonant tunneling through molecular orbitals [4, 34–36], enhanced current transport mediated by redox process [37, 38], interface related effects such as the presence of a strongly localized density of state at the electrode [39] or change of the interface dipole [40, 41] change in the molecule conformation [42, 43]. However, all these reports are concerned with the monolayer junctions or single molecule junctions and not with the multilayers as in the present work. Some exceptions are the works by Rampi and Whitesides groups on bilayer junctions incorporating molecules that suffer redox processes between the two organic monolayers [44], and results on bilayers of C_{60} molecules [45, 46]. In these C_{60} experiments, no NDR has been observed in the monolayer junction and a multilayer (2 or 3 in these reports) geometry seems to be a crucial requirement to observe NDR. In our case, a possible mechanism that explains the observed high current density and hysteretic effect in APTMS multilayers is as follows. We would like to point out that the observed hysteresis is intrinsic to the multilayers because of the following reasons: (i) the monolayer did not exhibit the hysteresis, (ii) a clear hysteresis was observed only for APTMS samples having ≥ 4-layers and (iii) the magnitudes of hysteresis and peak-to value ratio of NDR increased on increasing the number of layers. The first point also indicates that the hysteresis is not due to any effects occurring at multilayer/Si(p^{++}) and/or multilayer/Hg interfaces. We attribute the enhanced current density of the multilayers to be associated with the trapping of NH_3^+ ions. These trapped NH_3^+ ions in the multilayer are separated by approximately a length of monolayer, that is, ∼ 7 Å (see Fig. 6b). This distance is short enough to favor a hopping transport of the electrons through the NH_3^+ ion sites and, this explains why the multilayers exhibit much higher current than that expected from the tunneling mechanism.

The presence of NH_3^+ ions also qualitatively explains the observed hysteresis in the multilayers. It is well known that the gap between the highest occupied molecular (HOMO) and the lowest occupied molecular orbital (LUMO) for the alkyl-chains is ∼ 9 eV, making them electrically insulating. The presence of NH_3^+ ions creates localized states in the insulating gap. Thus, the observed hysteresis can be understood in terms of the Simmons and Verderber theory [47] of filling and de-filling of the traps created by positive ions in an insulator. In this theory, the electrons are assumed to move through the insulator by tunneling between adjacent impurity sites. The NH_3^+ positive ions – in order to satisfy the overall charge neutrality in the insulator – drag an equal number of electrons from the opposite electrode. Therefore, in the pristine state, when the bias is swept from $-V_{max} \rightarrow 0$ V, the current is low (i.e. high impedance state) as the traps are uncharged. In the positive bias region $0\ V \rightarrow +V_{max}$, the electrons get de-filled from the charge traps leading to a positive charging of the traps. As the bias is swept in the negative direction, i.e. $0\ V \rightarrow -V_{max}$, at low voltages the positive charge traps fill up with electrons, resulting in a high current (low impedance state). However, at high voltages, i.e. in the NDR region, electron filled charge traps create a space-charge field, which opposes the field applied at the injecting electrode and reduces the current which almost returns to the pristine state (high impedance state). The observed J–V hysteresis indicates that these multilayers are technologically important from the point of view of resistance random access memories, and therefore, gives room for further research.

4 Conclusions

We have deposited APTMS multilayers of varying thicknesses on SiO_2/Si(p^{++}) substrates using a self-assembly process. The mechanism of multilayer grafting was found to involve two different stages. In the first stage, APTMS monolayer chemisorbs on hydroxylated oxide surface by a silanization process and in the second stage, formation of a bilayer takes place as the surface amino group of the first monolayer chemisorbs the hydrolyzed silane group of another APTMS molecule. The second stage is a self-sustained process and results in the self-assembly of the multilayers with trapped NH_3^+ ions. The current–voltage characteristics of the multilayers exhibit a hysteresis effect along with a negative differential resistance, suggesting their potential application to molecular memory devices. A possible mechanism for the observed hysteresis effect based on filling and de-filling of the NH_3^+ traps has been discussed.

ACKNOWLEDGEMENTS This work was supported by the Indo-French Centre for the Promotion of Advanced Research (IFCPAR) through Project 3000-IT-1 and by the Indo-German Cooperation Programme (Project No: IND 06/005). We would like to thank Ms. N. Padma for developing Labview software for the J–V measurements and M. Senthilkumar, IIT Bombay, for analyzing the samples by XRD.

REFERENCES

1 D.K. Aswal, S. Lenfant, D. Guerin, J.V. Yakhmi, D. Vuillaume, Anal. Chim. Acta **568**, 84 (2006) and references therein
2 D. Vuillaume, J. Nanosci. Nanotechnol. **2**, 267 (2002)
3 S. Lenfant, C. Krzeminski, C. Delerue, G. Aallan, D. Vuillaume, Nano Lett. **3**, 741 (2003)
4 N.P. Guisinger, M.E. Greene, R. Basu, A.S. Baluch, M.C. Hersam, Nano Lett. **4**, 55 (2004)

5 Z. Liu, A.A. Yasseri, J.S. Lindsey, D.F. Bocian, Science **302**, 1543 (2003)
6 International Technology Roadmap for Semiconductors (IRTS), http://www.itrs.net/reports.html (2006)
7 J.B. Brzoska, I.B. Azouz, F. Rondelez, Langmuir **10**, 4367 (1994)
8 S.R. Wasserman, Y.-T. Tao, G.M. Whitesides, Langmuir **5**, 1074 (1989)
9 K. Kojio, S. Ge, A. Takahara, T. Kajiyama, Langmuir **14**, 971 (1998)
10 I. Doudevski, W.A. Hayes, D.K. Schwartz, Phys. Rev. Lett. **81**, 4927 (1998)
11 D.K. Schwartz, S. Steinberg, J. Israelachvili, J.A.N. Zasadzinski, Phys. Rev. Lett. **69**, 3354 (1992)
12 J. Collet, O. Tharaud, A. Chapoton, D. Vuillaume, Appl. Phys. Lett. **76**, 1941 (2000)
13 M. Halik, H. Klauk, U. Zschieschang, G. Schmid, C. Dehm, M. Schutz, S. Maisch, F. Effenberger, M. Brunnbauer, F. Stellacci, Nature **43**, 963 (2004)
14 D.K. Aswal, S. Lenfant, D. Guerin, J.V. Yakhmi, D. Vuillaume, Small **1**, 725 (2005)
15 R. Maoz, S. Matlis, E. DiMasi, B.M. Ocko, J. Sagiv, Nature **384**, 150 (1996)
16 R. Maoz, J. Sagiv, D. Degenhardt, H. Miihwald, P. Quint, Supramol. Sci. **2**, 9 (1995)
17 A. Wang, H. Tang, T. Cao, S.O. Salley, K.Y. Ng, J. Colloid Interf. Sci. **291**, 438 (2005)
18 R. Denoyel, J.C. Glez, P. Trens, Colloid Surf. A **197**, 213 (2002)
19 T.J. Horr, P.S. Arora, Colloid Surf. A **126**, 113 (1997)
20 A.V. Krasnoslobodtsev, S.N. Smirnov, Langmuir **18**, 3181 (2002)
21 G.C. Allen, F. Sorbello, C. Altavilla, A. Castorina, E. Ciliberto, Thin Solid Films **483**, 306 (2005)
22 D.F. Petri, G. Wenz, P. Schunk, T. Schimmel, Langmuir **15**, 4520 (1999)
23 D. Quere, Nature Mater. **1**, 14 (2002)
24 K.S. Taton, P.E. Guire, Colloid Surf. B **24**, 123 (2002)
25 N.P. Haung, R. Michel, J. Voros, M. Textor, R. Hofer, A. Rossi, D.L. Elbert, J.A. Hubbell, N.D. Spencer, Langmuir **17**, 489 (2001)
26 J. Chastain, R.C. King Jr. (Eds.), *Handbook of Photoelectron Spectroscopy* (Physical Electronics, Minnesota, USA, 1995), p. 57
27 H.L. Cabibil, V. Pham, J. Lozano, H. Celio, R.M. Winter, J.M. White, Langmuir **16**, 10 471 (2000)
28 S.M. Kanan, W.T.Y. Tze, C.P. Tripp, Langmuir **18**, 6623 (2002)
29 J. Beckmann, S.J. Grabowsky, Phys. Chem. A **111**, 2011 (2007)
30 G.S. Caravajal, D.E. Leyden, G.R. Quinting, G.E. Maciel, Anal. Chem. **60**, 1776 (1988)
31 M. Xu, D. Liu, H.C. Allen, Environ. Sci. Technol. **40**, 1566 (2006)
32 J.G. Simmons, J. Appl. Phys. **34**, 2581 (1963)
33 A. Salomon, D. Cahen, S.M. Lindsay, J. Tomfohr, V.B. Engelkes, C.D. Frisbie, Adv. Mater. **15**, 1881 (2003)
34 N.J. Tao, Phys. Rev. Lett. **76**, 4066 (1996)
35 T. Rakshit, G.C. Liang, A.W. Ghosh, S. Datta, Nano Lett. **4**, 1803 (2004)
36 Y. Karzazi, J. Cornil, J.L. Bredas, J. Am. Chem. Soc. **123**, 10 076 (2001)
37 R.A. Wassel, G.M. Credo, R.R. Fuierer, D.L. Feldheim, C.B. Gorman, J. Am. Chem. Soc. **126**, 295 (2004)
38 E. Tran, M.A. Rampi, G.M. Whitesides, Angew. Chem. Int. Edit. **43**, 3835 (2004)
39 Y. Xue, S. Datta, S. Hong, R. Reifenberger, J.I. Henderson, C.P. Kubiak, Phys. Rev. B **59**, R7853 (1999)
40 Y. Selzer, A. Salomon, J. Ghabboun, D. Cahen, Angew. Chem. Int. Edit. **41**, 827 (2002)
41 A. Salomon, R. Arad-Yellin, A. Shanzer, A. Karton, D. Cahen, J. Am. Chem. Soc. **126**, 11 648 (2004)
42 M.A. Reed, J. Chen, A.M. Rawlett, D.W. Price, J.M. Tour, Appl. Phys. Lett. **78**, 3735 (2001)
43 A. Blum, J.G. Kushmerick, D.P. Long, C.H. Patterson, J.C. Yang, J.C. Henderson, Y. Yao, J.M. Rour, R. Sashidhar, B.R. Ratna, Nature Mater. **4**, 167 (2005)
44 E. Tran, M. Duati, V. Ferri, K. Müllen, M. Zharnikov, G.M. Whitesides, M.A. Rampi, Adv. Mater. **18**, 1323 (2006)
45 C. Zeng, H. Wang, B. Wang, J. Yang, J.G. Hou, Appl. Phys. Lett. **77**, 3595 (2000)
46 M. Grobis, A. Wachowiak, R. Yamachika, M.F. Crommie, Appl. Phys. Lett. **86**, 204 102 (2005)
47 J.G. Simmons, R.V. Verderber, Proc. R. Soc. London **301**, 77 (1967)